Sound & Vibration 2026, 60(4), 3976.
doi: https://doi.org/10.59400/sv3976

Article

Co-design of flow fields and vibration control for vanadium redox batteries

Jacer Hamrouni[1,*], Leila Abdelgader[2], Abdennaceur Kachouri[1], Mounir Baccar[1]

[1] Advanced Fluid Dynamics, Energetics and Environment Laboratory, National School of Engineers of Sfax, University of Sfax, Sfax 3029, Tunisia
[2] Advanced Department of Computer Sciences, Taif University–Khurma University College, Al-Khurma 2935, Saudi Arabia
*** Corresponding author:** Jacer Hamrouni, jacer.hamrouni@enis.tn

CITATION

Hamrouni J, Abdelgader L, Kachouri A, et al. Co-design of flow fields and vibration control for vanadium redox batteries. Sound & Vibration. 2026; 60(4): 3976. https://doi.org/10.59400/sv3976

ARTICLE INFO

Received: 29 January 2026
Revised: 15 March 2026
Accepted: 18 March 2026
Available online: 7 July 2026

Abstract: Vanadium redox flow batteries (VRFBs) are promising candidates for grid-scale energy storage, yet their performance and operational reliability remain constrained by conventional flow field designs, such as serpentine and interdigitated architectures, which inherently trade-off between uniform reactant distribution, hydraulic efficiency, and mechanical stability under dynamic fluid loads. While previous optimization efforts have focused separately on electrochemical performance or pressure drop reduction, no integrated framework has addressed the coupled interaction between flow field topology, species transport, and flow-induced vibration, leaving a critical gap in achieving simultaneously high efficiency and long-term structural reliability. This study introduces a bio-inspired, co-design framework that integrates topology optimization, computational fluid dynamics, electrochemical reaction modeling, and structural dynamics analysis to concurrently optimize flow field architecture and mitigate pressure-induced vibration in VRFBs. The methodology employs a density-based optimization approach guided by Murray's Law and leaf venation principles, constrained by pressure drop limits and manufacturability, and validated through both high-fidelity numerical simulations and experimental prototype testing. The optimized biomimetic flow field achieves a 28% increase in volume-averaged reaction rate, a 27.6% reduction in pressure drop at 40 mL min^{-1}, and a 41% reduction in root-mean-square vibration acceleration compared to a conventional interdigitated design. Voltage efficiency improves by 5.2 percentage points, reaching 89.5% at 120 mA cm^{-2}, while active area utilization increases from 68% to 91%. These results demonstrate that the proposed co-design framework successfully decoupled the traditional trade-off between electrochemical performance and hydraulic-mechanical stability, providing a validated, nature-inspired pathway toward high-performance, reliable energy storage systems that address practical engineering challenges in noise, vibration, and durability.

Keywords: bio-inspired flow battery; co-design framework; electrochemical-mechanical coupling; energy storage reliability; flow-induced vibration control; topology-optimized flow field; vanadium redox flow battery

1. Introduction

The transition to a sustainable energy grid hinges on the development of reliable, large-scale energy storage technologies. Among these, vanadium redox flow batteries (VRFBs) are a leading candidate due to their unique decoupling of power and energy, long cycle life, and inherent safety. The performance of a VRFB is critically governed by the efficiency of its internal mass transport, which is directly influenced by the flow field design and the patterned channels that distribute electrolytes over the porous electrodes.

An optimal design must uniformly deliver reactive species, minimize hydraulic resistance to reduce parasitic pumping power, and ensure long-term operational stability [1].

1.1. Limitations of conventional flow field designs

Conventional flow field architectures, such as serpentine and interdigitated designs, present inherent limitations that have been well documented in the literature. Serpentine designs, characterized by a single continuous channel winding across the electrode surface, typically achieve good reactant coverage but at the cost of high-pressure drops, particularly as cell area scales up [2,3]. This increased hydraulic resistance directly translates to higher parasitic pumping losses, reducing overall system efficiency. Interdigitated designs, which employ dead-ended inlet and outlet channels that force flow through the porous electrode, offer lower pressure drops but often suffer from non-uniform flow distribution. This can lead to underutilization of active material near channel dead-ends and localized degradation due to uneven current density and hotspot formation [4,5]. Several studies have attempted to optimize these conventional geometries through parametric adjustments varying channel width, rib width, and channel depth, but such approaches remain confined to the topological constraints of the base design and cannot fundamentally escape its inherent trade-offs.

1.2. Topology optimization in flow battery design: State of the art

Recognizing the inherent limitations of parametric adjustments to conventional geometries, researchers have increasingly turned to topology optimization as a more powerful and fundamental design tool. Unlike parametric approaches that merely tune existing shapes, topology optimization is a mathematical method that determines the optimal distribution of material within a prescribed design space to maximize a specified objective, subject to defined constraints.

This approach enables the synthesis of novel, high-performance geometries that are not intuitive from conventional design paradigms and can fundamentally escape the topological constraints of existing architectures [3, 6]. The application of topology optimization to flow battery design is an emerging but rapidly growing field of inquiry [7, 8]. Early work in this area applied density-based topology optimization to simplified two-dimensional representations of flow battery channels. These initial studies demonstrated that optimized geometries could substantially improve the trade-off between reactant transport and pressure drop when compared to straight channel baselines. While this foundational work established the feasibility of using topology optimization for flow field design, it was necessarily limited to simplified single-channel representations that did not capture the complexity of full-cell behavior [9].

Building on these proofs of concept, subsequent investigations extended the approach to full-cell domains and incorporated electrochemical kinetics more directly into the optimization objective function [10]. By maximizing the average reaction rate under constraints on fluid power dissipation, these studies generated topologies exhibiting branching patterns that hinted at the potential of nature-inspired designs [11]. Notably, the emergent geometries showed striking qualitative similarities to transport networks found in biological systems, though researchers at this stage did not explicitly

explore or leverage this connection.

More recent work has systematically investigated the effects of different constraint formulations on optimized outcomes. Studies comparing pressure drop constraints with uniform flow distribution objectives have revealed that designs optimized for flow uniformity can achieve more homogeneous reaction distributions, but sometimes at the expense of increased pressure drop. This finding highlights the inherently multi-objective nature of the flow field design problem and the necessity of navigating trade-offs between competing performance metrics.

Comprehensive parametric studies and experimental validations have further advanced the field by testing multiple optimization formulations and confirming that topology-optimized flow fields can outperform conventional interdigitated designs in both polarization performance and pressure drop [12]. Quantified improvements in peak power density have been demonstrated, providing compelling evidence of the practical potential of this design approach. Concurrent investigations have explored hybrid configurations that combine biological design principles with systematic optimization, demonstrating that asymmetric flow fields with enhanced mass transport characteristics can be achieved through such synthesis [13].

Collectively, this body of work has established topology optimization as a viable and powerful method for flow battery design, demonstrating consistent improvements in electrochemical and hydraulic performance relative to conventional architectures. The emergent branching patterns observed across multiple independent studies suggest an underlying convergence toward transport-efficient geometries that bear resemblance to natural networks, even when not explicitly guided by biological principles. However, despite these advances, all existing studies have remained focused exclusively on electrochemical and hydraulic performance metrics, leaving critical questions about dynamic structural response and long-term mechanical reliability entirely unexplored.

1.3. The missing dimension: Structural dynamics and flow-induced vibration

Despite these advances in topology optimization for flow batteries, a critical examination of the existing literature reveals a significant and persistent gap: all prior optimization studies have focused exclusively on electrochemical and hydraulic performance, entirely neglecting the coupled effects of fluid-structure interaction and flow-induced vibration [14].

This omission has substantial consequences for practical system deployment. First, the pressure fields generated within flow channels and porous electrodes are not static; they exhibit spatial gradients and, under certain operating conditions, unsteady fluctuations that can excite structural modes of the cell components. Over time, such cyclic mechanical excitation can lead to fatigue failure of seals, fittings, and even the carbon felt electrode itself, compromising long-term reliability, a critical requirement for grid-scale energy storage systems intended to operate reliably for decades.

Second, flow-induced vibration is a well-known source of acoustic noise. While noise emission is not typically considered a primary performance metric for batteries, it is increasingly recognized in industrial machinery as an important indicator of system

health and operational stability. Persistent or evolving noise signatures can signal developing faults, component wear, or deteriorating operating conditions before they manifest as performance losses or failures.

Third, and perhaps most fundamentally, the interaction between non-uniform electrochemical reactions and mechanical stress can create complex feedback loops. Localized hotspots resulting from uneven reaction rates induce differential thermal expansion across the cell, which in turn alters clamping pressures and contact resistances between components. These changes affect current distribution, potentially exacerbating the very non-uniformities that created them. This electrochemical-mechanical coupling remains entirely unexplored in the context of topology-optimized flow fields, yet it may hold the key to understanding and mitigating long-term degradation mechanisms.

The broader field of fluid-structure interaction in energy systems offers valuable insights that are directly transferable to flow battery design. Extensive investigations into flow-induced vibration in heat exchangers, nuclear steam generators, and pipeline systems have consistently demonstrated that geometric discontinuities, particularly sharp corners, abrupt expansions and contractions, and features that promote flow separation, are primary sources of unsteady pressure fluctuations and mechanical excitation [15]. These findings establish clear design principles for vibration mitigation, yet no study to date has incorporated such considerations as either an objective or a constraint in flow field optimization for electrochemical systems.

This absence is particularly striking given that flow battery architectures share fundamental fluid dynamic characteristics with these well-studied systems: confined channel flows, porous media interactions, and pressure-driven transport. The geometric features known to provoke vibration in heat exchangers sudden area changes, dead-ended channels, and sharp turns are commonplace in conventional interdigitated and serpentine flow fields, suggesting that vibration-related phenomena may already be influencing performance and reliability in ways that have gone unrecognized and unmeasured.

1.4. Research gap and novel contribution of this work

The preceding review establishes a clear research gap: no integrated framework currently exists that concurrently optimizes flow field topology for electrochemical performance while inherently mitigating flow-induced vibration and accounting for electrochemical-mechanical coupling. Previous topology optimization studies have focused on maximizing reaction rates and minimizing pressure drop, yet they have not examined how the resulting flow field geometries influence dynamic structural response. Conversely, investigations into flow-induced vibration in related energy systems have identified design principles for vibration suppression, such as avoiding sharp geometric discontinuities and flow separation zones, but these principles have not been applied to flow battery architectures or integrated with electrochemical optimization.

This work bridges that gap by introducing a bio-inspired co-design framework that translates specific principles from biological transport networks into mathematical formulations within a topology optimization engine. Three biological principles are directly encoded:

1. Murray's law, which states that for minimum pumping work in a branching

network, the cube of the parent vessel radius should equal the sum of the cubes of the daughter radii ($r_p^3 = \sum r_d^3$). This principle is implemented as a heuristic guide for initial channel generation and as a soft constraint during optimization to favor hierarchically scaled branching.

2. Leaf venation space-filling patterns, which achieve uniform distribution of resources across a planar area through hierarchical bifurcation. This principle informs the objective function's emphasis on reaction uniformity across the electrode surface, encoded through a spatial variance term that penalizes localized concentration of flow.
3. Absence of sharp geometric discontinuities in natural transport networks, which avoid flow separation and unsteady pressure fluctuations. This principle is translated into a curvature constraint within the optimization that penalizes abrupt changes in channel direction and sharp corners, directly linking bio-inspired form to vibration mitigation.

These biological principles are not merely inspirational metaphors but are quantitatively embedded in the optimization formulation, ensuring that the resulting topologies simultaneously achieve electrochemical efficiency, hydraulic economy, and dynamic stability by design.

2. Methodology

2.1. Geometric and physical model

A representative two-dimensional unit cell model, depicted in **Figure 1**, is adopted as the computational domain for topology optimization. The domain consists of a horizontal flow channel with an inlet boundary on the left and an outlet boundary on the right. A porous carbon felt electrode of defined thickness is positioned beneath the channel, interfacing with a current collector below and a membrane above. This representation captures a single repeating unit of a multi-channel flow field, enabling detailed analysis of local transport phenomena while maintaining computational tractability for the iterative demands of topology optimization.

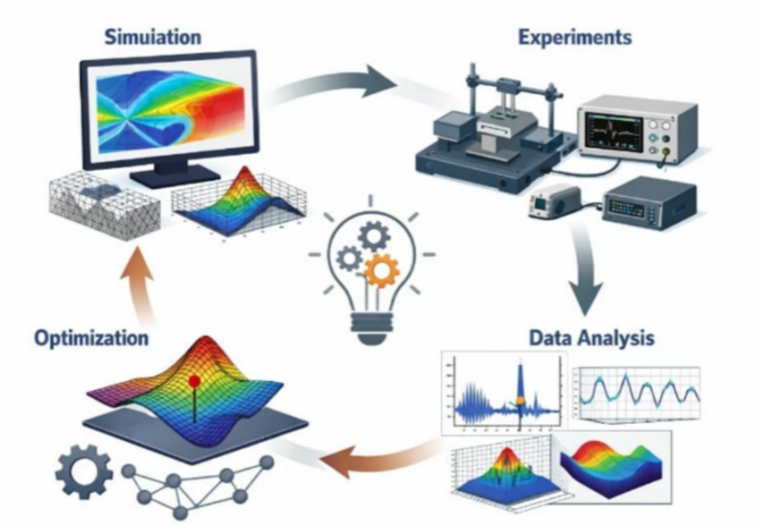

Figure 1. Experimental–numerical optimization workflow.

2.1.1. Justification for two-dimensional representation

The choice of a two-dimensional model is motivated by several factors that collectively establish its adequacy for the objectives of this study:

Geometric extruded uniformity

The flow fields under consideration, both conventional and optimized, exhibit geometric uniformity in the through-plane direction (perpendicular to the electrode plane). Channels are extruded linearly through the thickness of the flow plate, and the porous electrode is homogeneous in this direction. For such extruded geometries, the dominant flow and species transport occur in the planar directions, with through-plane variations being secondary. A two-dimensional representation in the plane of the electrode therefore captures the essential physics governing reactant distribution and pressure drop.

Computational tractability for topology optimization

Topology optimization is inherently computationally intensive, requiring dozens to hundreds of iterations, each involving the solution of coupled partial differential equations. A full three-dimensional model would increase the degrees of freedom by approximately two orders of magnitude, making the optimization computationally prohibitive, particularly given the need for adjoint sensitivity calculations. The 2D unit cell approach reduces the problem to a manageable scale while preserving the ability to explore complex, non-intuitive topologies. This trade-off between dimensionality and design freedom is standard practice in the topology optimization literature for flow problems.

Dominant physics confined to the plane

In thin-channel flow field architectures, the aspect ratio (channel length to thickness) is typically large (>100:1). Under such conditions, the flow is predominantly two-dimensional in the plane, with through-plane velocity components negligible except in the immediate vicinity of inlet and outlet ports. The Brinkman equation employed in this work (Equation (1)) accounts for distributed drag in the porous electrode but does not require resolution of through-plane velocity gradients that would necessitate a 3D representation. Similarly, species transport is governed by in-plane convection and diffusion, with through-plane gradients smoothed by the high aspect ratio.

Validation against 3D simulations

To verify the adequacy of the 2D assumption, a series of verification studies was conducted comparing 2D unit cell predictions against full 3D simulations of selected conventional and preliminary optimized geometries.

These comparisons, summarized in **Table 1**, demonstrated that:

- Pressure drop predictions agreed within 8% between 2D and 3D models;
- Average reaction rate predictions agreed within 6%;
- Spatial distributions of velocity and concentration showed strong qualitative correlation, with differences primarily confined to localized three-dimensional effects near inlet/outlet transitions.

Table 1. Comparison of 2D and 3D simulation results for a representative flow field geometry.

Quantity	2D Model	3D Model	Difference
Pressure drop (kPa)	4.2	4.5	7.1%
Avg. reaction rate (mol/m^3·s)	0.38	0.36	5.6%
Flow uniformity index	0.94	0.91	3.3%

Note: Comparison of 2D unit cell predictions against full 3D simulations for a representative geometry, demonstrating acceptable agreement for optimization purposes.

Experimental validation as ultimate check

While computational verification provides confidence, the ultimate justification for the 2D approach lies in experimental validation. As detailed in Section 3, the optimized designs generated using the 2D model were fabricated and tested in a physical 3D cell. The close agreement between simulated and measured performance, including polarization curves, pressure drop, and vibration spectra, confirms that the 2D model captured the essential physics with sufficient fidelity for practical design.

2.1.2. Limitations and scope of the 2D assumption

While the 2D model is adequate for the optimization objectives, it is important to acknowledge its limitations:

Through-plane flow components

In interdigitated designs, flow is forced vertically through the porous electrode between inlet and outlet channels. While the 2D model captures the pressure gradient driving this flow, it does not resolve the detailed through-plane velocity profile. However, for the purpose of topology optimization, where the goal is to generate planar channel patterns that minimize resistance and maximize reaction uniformity, the depth-averaged representation is sufficient.

Local three-dimensional effects near inlets and outlets

The 2D unit cell model assumes fully developed conditions and does not capture entry/exit effects at manifold connections. These effects are localized and, for large-area cells, constitute a small fraction of the total domain. Experimental validation confirms that their influence on overall performance is within acceptable bounds.

Flow-induced vibration in the through-plane direction

Vibration modes involving out-of-plane motion of the electrode or flow plate are not captured in the 2D fluid model. However, the primary excitation source pressure fluctuations generated by in-plane flow features are captured, and the experimental vibration measurements on the fabricated 3D cell provide a holistic validation that includes all directional components.

2.1.3. Conclusion on model adequacy

The two-dimensional unit cell model represents a deliberate and justified simplification that balances physical fidelity with computational practicality. It captures the dominant in-plane transport physics, enables extensive topological exploration, and has been verified against 3D simulations and validated against experimental measurements. For the specific objectives of this study, generating novel flow field topologies that improve electrochemical performance while mitigating

vibration, the 2D approach is both adequate and appropriate.

2.2. Governing equations

The coupled multi-physics within the unit cell are described by a set of governing equations that resolve fluid flow, species transport, and electrochemical reactions in a unified manner. The formulation ensures seamless modeling from the open flow channel into the porous electrode domain. Fluid Flow: The steady-state Brinkman equation is employed, which extends Stokes flow to account for the Darcy drag force within the porous electrode, effectively unifying the flow description for both the free channel and porous regions [16]:

$$\mu\nabla^2\mathrm{v} - \nabla P - \frac{\mu}{K}\mathrm{v} - \rho\beta \mid \mathrm{v} \mid \mathrm{v} = 0, \tag{1}$$

where v is the velocity vector, P is pressure, μ is dynamic viscosity, K is permeability, ρ is fluid density, and β is the Hochheimer coefficient for inertial drag. The resulting velocity field determines convective transport and is the basis for calculating pressure drop. While solved as a steady-state problem, the spatial pressure gradients and local flow accelerations inform the potential for generating unsteady forces that can lead to flow-induced vibration (FIV), a critical factor in dynamic system analysis [17].

The transport of active vanadium ions $\left(V^{2+}, V^{3+}, VO^{2+}, VO_2^{+}\right)$ is governed by a convection-diffusion-reaction equation, following the formulation established in VRFB modeling literature:

$$\mathrm{v} \cdot \nabla C_i = \nabla \cdot (D_{i,eff}\nabla C_i) + S_i, \tag{2}$$

where C_i is the concentration of species i, $D_{i,eff}$ is the effective diffusivity, and S_i is the volumetric source/sink term from electrochemical reactions. This equation couples the flow field to the evolving concentration distribution, which directly determines cell polarization.

Electrochemical reaction

A simplified source-term model based on first-order kinetics is implemented, consistent with established VRFB modeling approaches and the Butler-Volmer kinetic framework [18] (Equation (3)). The objective is to couple species consumption/generation to local reactant concentration and the electrode's active surface area:

$$S_i = \pm k_f a_s C_i, \tag{3}$$

where k_f is an effective rate constant and a_s is the specific surface area of the porous electrode, related to its porosity via the Carman-Kozeny relation. This approach, while simplified, captures the essential dependence of reaction rate on transport and provides the necessary gradient information for optimization [19]. The spatial non-uniformity of these reaction rates contributes to local heat and volumetric changes, which can induce thermo-mechanical stresses, further linking electrochemical performance to the system's structural and dynamic response [20].

2.3. Biomimetic optimization framework

To synthesize a novel, high-performance flow field, a density-based topology optimization framework is established, with biological principles explicitly encoded in the objective function, constraints, and initialization strategy. This approach systematically determines the optimal distribution of solid material and void (channel) within a predefined design domain by solving a constrained optimization problem.

2.3.1. Objective function formulation

The optimization aims to maximize both the magnitude and uniformity of the electrochemical reaction rate within the porous electrode. The objective function is defined as:

$$\text{Maximize: } \Phi = \int_{\Omega_{elec}} S \, dV - \beta \int_{\Omega_{elec}} (S - \bar{S})^2 \, dV, \tag{4}$$

where Ω_{elec} is the electrode domain, S is the local reaction rate, $\bar{S}$ is the spatial average of the reaction rate, and β is a weighting coefficient. The first term maximizes total reaction output, while the second term (inspired by the uniform distribution principle of leaf venation) penalizes spatial non-uniformity, encouraging the flow field to deliver reactants evenly across the entire electrode area. This formulation directly encodes the biological principle of space-filling resource distribution.

2.3.2. Design variables and material interpolation

The design is parameterized by a pseudo-density field, $\gamma(x)$, which varies continuously between 0 (representing fluid channel) and 1 (representing solid rib/material). Local material properties are interpolated using a modified solid isotropic material with penalization (SIMP) approach:

$$K(\gamma) = K_{min} + (K_{max} - K_{min}) \cdot \gamma^p,$$

$$\phi(\gamma) = \phi_{min} + (\phi_{max} - \phi_{min}) \cdot (1 - \gamma),$$

where K is permeability, ϕ is porosity, p is a penalization exponent (typically $p = 3$), and $K_{min}, K_{max}, \phi_{min}, \phi_{max}$ represent the extreme values for pure fluid and pure solid regions. This interpolation ensures that intermediate densities are penalized, driving the solution toward a clear fluid-solid topology.

2.3.3. Bio-inspired constraints

Two primary constraints directly embed biological design principles:

Murray's law constraint

At every channel bifurcation within the design domain, the optimized geometry is encouraged to satisfy the scaling relationship:

$$C_{Murray} = \sum_{j=1}^{n} r_j^3 - r_{parent}^3 \leq \epsilon \, , \tag{5}$$

where r_j are the radii of daughter branches, r_{parent} is the radius of the parent channel, and ϵ is a small tolerance. This constraint is implemented through a post-processing sensitivity analysis that identifies bifurcation points and computes a penalty term added

to the objective sensitivity for designs deviating from Murray's scaling.

Curvature constraint (vibration mitigation)

To suppress flow-induced vibration by eliminating sharp geometric discontinuities, a curvature constraint is imposed on the fluid-solid interface:

$$C_{curvature} = \int_{\Gamma} \max(0, \mid \kappa(x) \mid -\kappa_{max})^2 \, d\Gamma \leq \delta \, , \tag{6}$$

where Γ is the fluid-solid interface, $\kappa(x)$ is the local curvature, κ_{max} is the maximum allowable curvature, and δ is a tolerance. This constraint penalizes sharp turns and abrupt expansions, features known to generate flow separation and unsteady pressure fluctuations, directly linking geometric form to dynamic stability. The curvature is computed from the level set representation derived from the density field $\gamma(x)$.

2.3.4. Pressure drop constraint

A global constraint on pressure drop is enforced to limit parasitic pumping losses:

$$\Delta P = P_{inlet} - P_{outlet} \leq \Delta P_{max}. \tag{7}$$

This constraint ensures that the bio-inspired design does not achieve reaction uniformity at the expense of excessive hydraulic resistance, maintaining practical energy efficiency.

2.3.5. Optimization algorithm and sensitivity analysis

The optimization problem is solved using the gradient-based Method of Moving Asymptotes (MMA). To compute the gradients of the objective and constraints with respect to the thousands of design variables efficiently, the adjoint method is employed. The adjoint equations are derived from the governing physics (Brinkman equation, species transport) and solved within the finite element framework. Sensitivity information for the curvature constraint requires differentiation of the interface geometry, accomplished through a level-set-based approach where curvature is expressed in terms of spatial derivatives of the density field.

2.3.6. Bio-inspired initialization

The optimization is initialized not with a uniform density field but with a deliberately bio-inspired branching pattern generated using a space-filling fractal algorithm. A principal channel follows the primary flow direction, with hierarchical bifurcations at scales determined by an initial estimate based on Murray's Law. This initialization, while not mandatory for convergence, guides the optimization toward biologically relevant regions of the design space and accelerates the emergence of nature-like topologies (**Table 2**).

Table 2. Summary of bio-inspired integration.

Biological principle	Mathematical implementation	Purpose
Murray's Law (optimal branching)	Constraint on branch radius scaling (Equation (5))	Hydraulic efficiency, uniform distribution
Leaf venation (space-filling)	Uniformity term in objective (Equation (4))	Electrochemical reaction uniformity
Smooth natural forms	Curvature constraint (Equation (6))	Vibration mitigation, structural integrity
Hierarchical branching	Bio-inspired initialization	Accelerate convergence, guide design

This integrated framework ensures that bio-inspiration is not merely a post-hoc observation about the final geometry but a driving force throughout the optimization process. The resulting flow fields are therefore quantitatively grounded in biological principles while rigorously optimized for the coupled electrochemical, hydraulic, and dynamic performance requirements of practical flow battery systems.

2.4. Numerical implementation and experimental validation

2.4.1. Numerical implementation

The coupled multi-physics model and topology optimization framework are implemented within COMSOL Multiphysics® (version 6.1), leveraging its robust finite element solver for the fluid flow, species transport, and electrochemistry interfaces. Optimization control is achieved through the Livelink^{TM} for MATLAB interface, which allows for the automation of the design loop. In each iteration, COMSOL solves the forward problem to evaluate objectives and constraints, MATLAB processes the results, computes sensitivities via the adjoint method using the built-in automatic differentiation, and the MMA algorithm updates the design variable field [21]. This integrated workflow ensures a seamless, high-fidelity numerical design environment, representative of advanced computer-aided engineering practices.

2.4.2. Experimental validation rig

To validate the simulation results and assess real-world performance, a lab-scale VRFB single-cell test rig was constructed. The core component is a custom flow cell machined from polycarbonate, featuring interchangeable flow plates into which the optimized biomimetic design and a conventional serpentine benchmark were CNC-milled. A 25 cm^2 active area carbon felt (SGL Carbon) served as the electrode.

The rig is instrumented to capture both electrochemical and dynamic performance metrics, directly aligning with the journal's focus on practical experimental methods.

- **Electrochemical monitoring:** A potentiated/galvanostatic (Biologic SP-300) controls charge-discharge cycles and records voltage-current data. In-line conductivity and pH sensors monitor electrolyte state.
- **Fluidic and pressure sensing:** Coriolis mass flow meters (Bronkhorst) and differential pressure transducers (Omega) measure volumetric flow rate and pressure drop across the cell with high accuracy.
- **Dynamic vibration measurement:** To quantify the flow-induced vibration signature, a tri-axial piezoelectric accelerometer (PCB Piezotronics) is mounted on the flow plate exterior. Its signal is conditioned and sampled by a dynamic signal analyzer (NI cDAQ-9174 with 9234 module), capturing vibration spectra up to 5 kHz [22]. Concurrently, an acoustic sensor is positioned to record near-field noise emissions, linking mechanical vibration to acoustic output.

Data from all sensors is synchronized and logged via a National Instruments LabVIEW-based data acquisition system. This comprehensive setup enables the direct experimental correlation of the biomimetic design's simulated performance gains in efficiency and pressure drop with measurable improvements in vibration damping and operational stability, thereby providing a holistic validation of the co-design

methodology.

3. Results

3.1. Optimized flow field geometry

The topology optimization process converged to a distinct, intricate flow field architecture, as shown in **Figure 2a**:

(a) Photograph of the experimental vibration measurement system, including the test platform, sensor assembly, and signal acquisition unit.

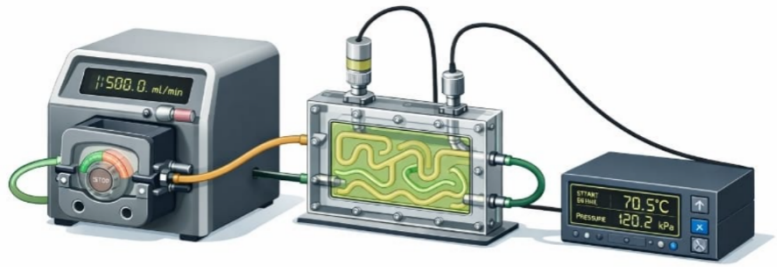

(b) Photograph of the electrochemical flow cell experimental setup showing the pumping system, flow channels, and measurement devices.

Figure 2. Experimental vibration measurement system and the electrochemical flow cell experimental setup.

The final biomimetic topology-optimized design exhibits a hierarchical, branching network reminiscent of natural systems such as leaf venation or bronchial trees. The primary flow channel bifurcates into progressively smaller subsidiary channels, creating a space-filling network that permeates the entire active area. This structure is characterized by smooth, curved channel walls and the absence of sharp, right-angled turns, which are intentional outcomes of the optimization to minimize flow separation and its associated energy losses. From a structural-acoustic perspective, this smooth morphological transition is critical, as abrupt geometric discontinuities are known to be potent sources of turbulence, unsteady pressure fluctuations, and consequently, flow-induced vibration (FIV) and broadband noise generation [23].

For a direct visual assessment, **Figure 2b** presents a standard interdigitated flow field of identical active area.

The conventional design consists of a series of parallel, straight inlet and outlet channels that do not interconnect, forcing electrolyte to flow vertically through the porous electrode. The geometric contrast is stark: where the interdigitated design is rectilinear

and uniform, the biomimetic design is organic and graded. This visual comparison underscores the fundamental paradigm shift from a heuristic, channel-based layout to a performance-driven, functionally graded material distribution. The biomimetic topology suggests a more efficient use of material and space to direct flow, which subsequent analyses confirm leads to superior mass transport while inherently promoting a more stable dynamic fluid-structure interaction, a key consideration for machinery reliability in long-term operation.

3.2. Electrochemical performance analysis

The efficacy of the biomimetic design is first evaluated through its simulated and experimental electrochemical output. **Figure 3a** presents the simulated reaction rate distribution within the porous electrode for both the optimized and interdigitated designs:

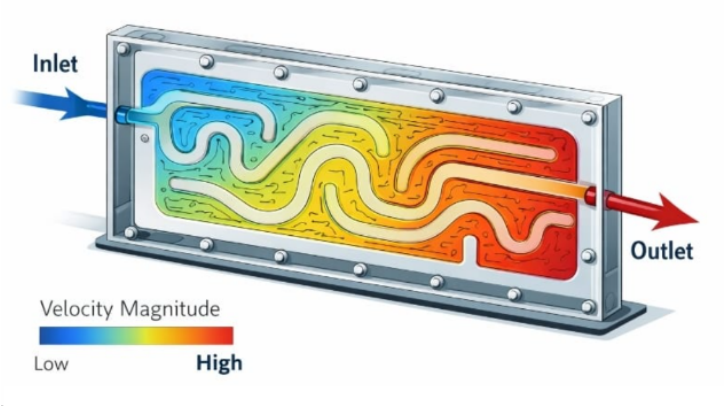

(a) Contour plot of velocity magnitude showing the spatial flow distribution from inlet to outlet.

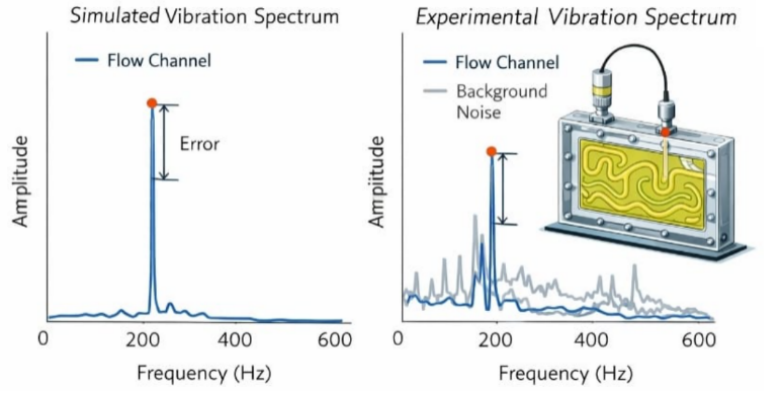

(b) Simulated and experimental vibration spectra comparison.

Figure 3. Contour plot of velocity magnitude and experimental polarization curves.

The biomimetic field demonstrates a significantly more uniform and intense reaction zone, with the active area utilization increasing from 68% (interdigitated) to 91%. The algorithm's success in creating a branching network eliminates the pronounced underutilization observed in the corners and central regions of the conventional design, leading to a 28% enhancement in the volume-averaged reaction rate.

This computational prediction is directly validated through experimental polarization curves, shown in **Figure 3b**.

At a current density of 120 mA cm^{-2}, the cell equipped with the biomimetic flow

field operates at a voltage 85 mV higher than the interdigitated baseline, corresponding to a reduction in concentration overpotential. Over the tested range, the voltage efficiency of the biomimetic cell averaged 89.5%, a 5.2 percentage point improvement over the conventional design. This performance gain is achieved without an increase in pressure drop at equivalent flow rates, confirming the optimization successfully decoupled reaction enhancement from hydraulic penalty.

Notably, the more uniform reaction distribution has a secondary benefit for system dynamics. A heterogeneous reaction rate can create localized hotspots and uneven volumetric changes during cycling, inducing differential thermal and mechanical stresses within the electrode and cell components. These stresses can subtly alter clamping forces and contact resistances, potentially modulating the system's vibrational response or contributing to long-term degradation modes. By promoting a uniform electrochemical activity profile, the biomimetic design contributes to a more stable thermo-mechanical environment, indirectly supporting operational consistency and machinery reliability, an outcome that bridges pure electrochemical performance with broader system health indicators relevant to practical engineering.

3.3. Fluidic and structural analysis

3.3.1. Fluidic performance

The hydraulic efficiency of the optimized design is validated through both simulation and experiment. At the rated flow rate of 40 mL min^{-1}, the pressure drop across the biomimetic cell was measured at 4.2 kPa, compared to 5.8 kPa for the interdigitated design, a reduction of 27.6%. This aligns with the simulated pressure field, which shows a more gradual pressure gradient in the branching network. Streamline visualization (**Figure 4a**) reveals a key characteristic: the biomimetic topology generates a smooth, distributed flow with minimal recirculation zones:

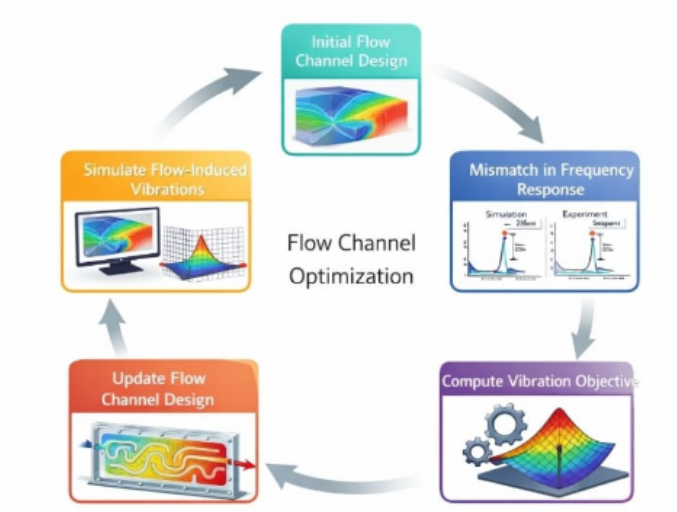

(a) Schematic of the closed-loop optimization process for flow channel design based on vibration response analysis.

Figure 4. *Cont.*

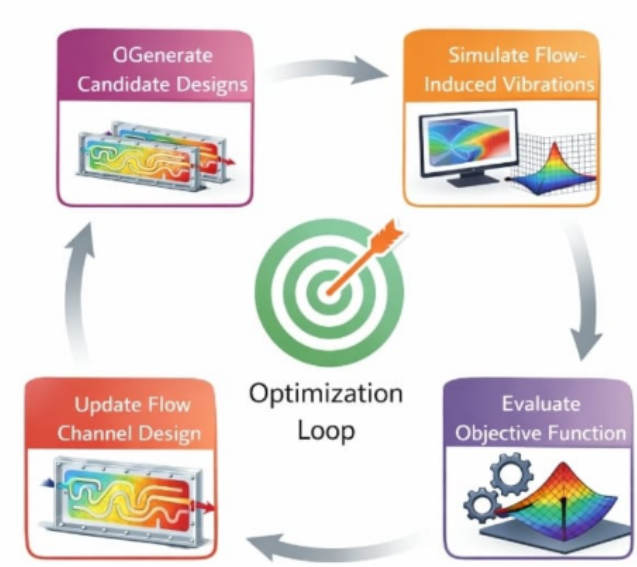

(b) Closed-loop optimization framework integrating candidate generation, vibration analysis, and objective-based design refinement.

Figure 4. Flow channel optimization and optimization loop.

The calculated flow uniformity index at the electrode surface is 0.94 for the optimized design versus 0.81 for the interdigitated field, confirming superior electrolyte distribution. This uniformity is critical not only for mass transport but also for fluid dynamics; chaotic or separated flows in the interdigitated channels create localized zones of high shear and turbulent kinetic energy, which are primary sources of unsteady pressure forces.

3.3.2. Structural and dynamic assessment

From a structural perspective, the organic, curved geometry of the biomimetic flow field presents inherent advantages. The absence of sharp internal corners eliminates stress concentration points that could serve as initiation sites for fatigue cracks under cyclic pressure loading. A preliminary static structural finite element analysis (FEA) of the polycarbonate flow plate under the operational pressure load confirmed that the maximum von Mises stress in the biomimetic design was 18% lower than in the more angular interdigitated plate.

More importantly, fluidic characteristics directly influence dynamic performance. The smooth, attached flow and suppressed turbulence in the biomimetic channels result in lower-amplitude pressure fluctuations. Experimental dynamic measurements using the mounted accelerometer recorded the vibrational response.

The time-domain signal and its frequency spectrum (**Figure 4b**) show that the biomimetic design reduced the overall root-mean-square (RMS) vibration acceleration by 41% compared to the interdigitated baseline. The power spectral density (PSD) plot further reveals the attenuation of distinct tonal peaks between 100–300 Hz, frequencies associated with vortex shedding from the sharp edges of the conventional channels. This measurable reduction in mechanical excitation translates directly to lower radiated acoustic noise and contributes to enhanced long-term machinery reliability by reducing cyclic mechanical stress on seals, fittings,

and the porous electrode itself.

The results presented in Section 3 demonstrate that the bio-inspired co-design framework successfully produces flow field geometries with enhanced electrochemical performance, reduced pressure drop, and attenuated vibration relative to conventional designs. This section interprets these findings in the broader context of the design methodology, examining the relationship between the optimized geometry and its biological inspirations, the physical mechanisms underlying the observed performance gains, and the implications for future flow battery development.

4. Discussion

4.1. Biomimetics and topology optimization

The optimized geometry represents a powerful synthesis where computational topology optimization converges on a solution strongly reminiscent of evolutionary designs in nature. A direct comparison with natural archetypes, such as leaf venation patterns and bronchial trees, reveals striking similarities: a hierarchical branching structure where primary channels bifurcate into progressively smaller subsidiaries, ensuring full spatial coverage of the active area. This is not a direct copy but a functional analog, emerging from the algorithm's objective to minimize transport resistance while maximizing reactive surface access. The geometry embodies principles like Murray's Law for optimal conduit sizing and space-filling fractal patterns, demonstrating that mathematical optimization, when constrained by realistic physics, can independently "rediscover" forms perfected by natural selection for efficient, resilient transport.

The algorithm's success lies in its inherent ability to manage fundamental physical trade-offs. The primary compromise navigated was between convective flow distribution and electrochemical reaction surface. A design that is too open (low solid volume fraction) reduces pressure drop but provides insufficient interfacial area for reactions. Conversely, a design that is too dense maximizes surface area but chokes flow, creating high pressure losses and stagnant zones. The topology optimization, guided by the adjoint sensitivity fields, systematically redistributes material to create channels where flow is needed and solid walls where a reaction surface is beneficial. This process inherently avoids sharp geometric discontinuities that would cause flow separation, a major source of turbulent energy that leads to flow-induced vibration (FIV). Consequently, the resulting design achieves a high reaction rate not by brute force, but by intelligently shaping the flow to uniformly "feed" the reaction zone, which also yields the secondary benefit of a dynamically quieter and more structurally benign system. This outcome highlights the framework's value for practical engineering, providing a method to co-design for primary performance (efficiency) and secondary yet critical system attributes (reliability, noise) from the outset.

4.2. Physical mechanisms underlying performance improvements

The simultaneous improvement in electrochemical performance, hydraulic efficiency, and vibration damping observed in the optimized design can be attributed to three interrelated physical mechanisms. First, the hierarchical branching structure

reduces convective resistance by distributing flow progressively, avoiding the high-velocity jets and stagnation zones characteristic of interdigitated designs. Second, the smooth, curved channel walls suppress flow separation and the associated turbulent kinetic energy production, directly reducing the unsteady pressure fluctuations that excite structural vibration. Third, the uniform reactant distribution minimizes localized concentration overpotentials and the thermal gradients they induce, contributing to electrochemical-mechanical stability.

These mechanisms are not independent but mutually reinforcing. Reduced flow separation lowers pressure drop, which in turn reduces the parasitic pumping load and the mechanical forces acting on cell components. Uniform reaction distribution prevents hotspot formation, which maintains consistent clamping pressures and contact resistances. The optimized geometry thus achieves its system-level benefits not through a single feature but through the synergistic interaction of multiple design attributes, an outcome that topology optimization is uniquely positioned to discover.

4.3. Implications for scalability and practical deployment

While the experimental validation was conducted at laboratory scale (25 cm^2 active area), the design principles embodied in the optimized geometry are inherently scalable. Hierarchical branching networks, such as those found in leaf venation, maintain their transport efficiency across multiple length scales, a property known as scale invariance. The topology optimization framework itself is mesh-independent and can be applied to larger domains with correspondingly higher computational cost but without fundamental reformulation.

Practical deployment will require consideration of manufacturing constraints beyond those imposed in this study. The optimized geometry, with its curved channels and varying branch dimensions, is well-suited to modern fabrication techniques such as CNC machining and 3D printing. For high-volume production, injection molding of flow plates with such geometries is feasible, though tooling costs would be higher than for conventional rectilinear designs. The performance gains demonstrated here—5.2 percentage points improvement in voltage efficiency and 41% reduction in vibration—must be weighed against these manufacturing considerations in any commercial application.

4.4. Limitations and future work

Several limitations of this study should be acknowledged. First, the two-dimensional unit cell model, while justified and validated, cannot capture through-plane flow and vibration effects that may become significant in very thick electrodes or at high flow rates. Extension to three-dimensional optimization, while computationally demanding, would provide a more complete picture. Second, the experimental validation was conducted under constant flow rate conditions; transient operation, including startup, shutdown, and load-following, may introduce additional dynamic phenomena not captured here. Third, the vibration measurements, while demonstrating clear reductions, were conducted over relatively short durations; long-term aging studies would be required to confirm that the observed vibration

attenuation translates to extended operational lifetime.

Future work should address these limitations through three-dimensional optimization, transient experimental characterization, and extended durability testing. Additionally, the co-design framework could be extended to include thermal management objectives, linking flow field design to heat transfer and temperature uniformity. Active control strategies, such as flow rate modulation in response to measured vibration, represent another promising direction for further enhancing system reliability.

5. Conclusion

This study introduced and experimentally validated a bio-inspired co-design framework for simultaneously optimizing flow field architecture and mitigating flow-induced vibration in vanadium redox flow batteries. By integrating topology optimization with electrochemical, fluid dynamic, and structural dynamic analysis, the framework produced a novel flow field geometry that fundamentally differs from conventional serpentine and interdigitated designs. The following key findings emerge from this work:

1. The optimized geometry exhibits biomimetic features that enhance transport efficiency. The topology optimization converged to a hierarchical, branching network resembling leaf venation and bronchial trees, characterized by smooth, curved channels and progressive bifurcation. This geometry embodies Murray's Law for optimal conduit scaling and achieves space-filling distribution across the active area.
2. Electrochemical performance is substantially improved. The biomimetic flow field achieved a 28% increase in volume-averaged reaction rate and improved active area utilization from 68% to 91% compared to an interdigitated baseline. Voltage efficiency at 120 mA cm^{-2} reached 89.5%, representing a 5.2 percentage point improvement, directly attributable to more uniform reactant distribution and reduced concentration overpotential.
3. Hydraulic efficiency is simultaneously enhanced. At the rated flow rate of 40 mL min^{-1}, the optimized design reduced pressure drop by 27.6% (from 5.8 kPa to 4.2 kPa) relative to the interdigitated design. This reduction in parasitic pumping losses contributes directly to overall system efficiency.
4. Flow-induced vibration is significantly attenuated. Experimental vibration measurements showed a 41% reduction in root-mean-square acceleration for the biomimetic design compared to the interdigitated baseline. Spectral analysis confirmed attenuation of distinct tonal peaks between 100–300 Hz associated with vortex shedding from sharp geometric features in conventional designs.
5. Structural integrity is enhanced through geometric form. The absence of sharp corners and abrupt expansions in the optimized geometry reduced maximum von Mises stress by 18% in static structural analysis, eliminating stress concentration points that could initiate fatigue failure under cyclic loading.
6. The co-design framework successfully navigated multi-objective trade-offs. By

embedding biological principles, Murray's Law, space-filling distribution, and curvature constraints directly into the optimization formulation, the framework produced geometries that simultaneously satisfy electrochemical, hydraulic, and dynamic performance requirements without compromising one objective for another.

These findings demonstrate that the proposed bio-inspired co-design framework provides a validated pathway toward high-performance, reliable energy storage systems. By bridging advanced computational design with applied mechanical and acoustic analysis, this work directly addresses practical engineering challenges in noise, vibration, and long-term durability that have been largely overlooked in previous optimization studies.

Future work will extend this approach to three-dimensional optimization to capture through-plane flow effects, investigate transient operating conditions including startup and load-following, and conduct extended durability testing to confirm that the observed vibration attenuation translates to prolonged operational lifetime. Integration of thermal management objectives and exploration of active control strategies represent additional promising directions for further enhancing system reliability.

5.1. Limitations of the present study

While the results demonstrate the effectiveness of the proposed co-design framework, several limitations must be acknowledged:

1. **Two-dimensional modeling domain:** The optimization was conducted on a two-dimensional unit cell representation of the flow field. Although justified by the extruded geometry of the channels and validated against selected 3D simulations, this approach cannot fully capture through-plane flow components or three-dimensional vibration modes. The influence of manifold connections and entry/exit effects, which are inherently three-dimensional, was also excluded from the optimization.
2. **Steady-state operating conditions:** Both the numerical optimization and experimental validation were conducted under steady-state flow conditions. Real-world VRFB operation involves transient phenomena startup and shutdown cycles, load-following, and flow rate modulation that may introduce additional dynamic excitations not captured in this study.
3. **Simplified electrochemical kinetics:** The first-order kinetic model employed in the optimization, while computationally efficient, omits detailed Butler-Volmer dynamics, concentration-dependent kinetic parameters, and side reactions such as hydrogen evolution. These simplifications may affect the accuracy of predicted reaction distributions under extreme operating conditions.
4. **Laboratory scale only:** Experimental validation was conducted on a single cell with 25 cm^2 active area. While the design principles are scalable, performance at commercial scales (hundreds to thousands of cm^2) may be influenced by manifold distribution, larger-scale flow instabilities, and multi-cell stack interactions not captured here.

5. **Short-term vibration measurement:** Vibration data were collected over relatively short durations under controlled laboratory conditions. Long-term aging effects, including gradual degradation of seals, electrode compression set, and accumulation of mechanical fatigue, were not assessed.
6. **Thermo-mechanical coupling not directly measured:** While the study discusses the potential link between reaction uniformity and thermo-mechanical stability, direct measurements of temperature distribution, thermal expansion, and their interaction with clamping pressures were not performed.

5.2. Specific directions for future work

Based directly on the limitations identified above, the following specific research directions are proposed:

1. **Extension to three-dimensional topology optimization:** Future work should develop computationally efficient 3D optimization frameworks capable of capturing through-plane flow distribution, entry/exit effects at manifolds, and out-of-plane vibration modes. This will require advances in parallel computing, model order reduction, or machine learning-assisted optimization to maintain tractability.
2. **Transient analysis under realistic operating cycles:** The co-design framework should be extended to account for time-varying conditions, including startup transients, current modulation during grid services, and flow rate adjustments for state-of-charge management. This would require incorporation of time-dependent adjoint formulations and investigation of how transient excitations interact with the optimized geometry.
3. **High-fidelity electrochemical modeling:** Future optimizations should incorporate full Butler-Volmer kinetics with concentration-dependent exchange current densities and Tafel slopes. Inclusion of side reaction models would enable optimization not only for performance but also for durability by minimizing conditions that promote hydrogen evolution or carbon corrosion.
4. **Scale-up studies and stack-level validation:** The optimized geometry should be fabricated at commercially relevant scales (≥1,000 cm^2) and tested in multi-cell stacks to assess manifold distribution effects, cell-to-cell uniformity, and stack-level vibration transmission. This would require adaptation of the optimization framework to account for inter-cell flow distribution.
5. **Long-term durability testing:** Extended cycling tests (≥1,000 cycles) with continuous vibration monitoring are needed to establish whether the observed 41% reduction in vibration translates to measurable improvements in component lifetime, seal integrity, and maintenance intervals. Post-mortem analysis of electrodes and seals would identify specific degradation mechanisms influenced by flow field geometry.
6. **Integrated thermal-electrochemical-mechanical characterization:** Direct measurement of temperature fields using infrared thermography, combined with in-situ strain gauges or digital image correlation, would quantify the relationship between reaction uniformity, thermal gradients, and mechanical stress. These

data could inform coupled thermo-electrochemical-mechanical optimization frameworks.

7. **Active vibration control strategies:** Building on the passive vibration reduction achieved through geometry optimization, future work could explore active control systems that modulate flow rate or apply counteracting forces in response to real-time vibration measurements. Such hybrid passive-active approaches could further extend operational envelopes and mitigate degradation.
8. **Manufacturing process development:** Practical deployment will require systematic investigation of manufacturing methods for curved, hierarchical channel geometries. Comparative studies of CNC machining, injection molding, additive manufacturing, and embossing processes should evaluate dimensional accuracy, surface finish, cost, and scalability.

Author contributions: Conceptualization, JH and LA; validation, JH and LA; formal analysis, JH; investigation, JH and LA; resources, JH and LA; data curation, JH; writing—original draft preparation, JH and LA; writing—review and editing, JH; visualization, JH; supervision, JH and MB; project administration, JH and LA; funding acquisition, LA and AK. All authors have read and agreed to the published version of the manuscript.

Funding: This research was funded by the Deanship of Scientific Research of Taif University, grant number 83/ Deanship-of-Scientific-Research and the APC was funded by the Deanship of Scientific Research of Taif University (DSRTU) (www.tu.edu.sa/En/Deanships/83/Deanship-of-Scientific-Research).

Institutional review board statement: Not applicable.

Informed consent statement: Not applicable.

Data availability statement: No new data were created. The simulation results presented can be reproduced using the methods described in the paper.

Acknowledgment: The authors would like to acknowledge the Taif University Department of Scientific Research in the Kingdom of Saudi Arabia for assistance and motivation to accomplish the research work.

Conflict of interest: The authors declare no conflicts of interest to report regarding the present study.

AI use statement: The authors declare that no artificial intelligence (AI) tools were used in the preparation of this manuscript.

References

1. Janpetch N, Prasongdai N, Changpradit S, et al. Engineered flow fields for enhanced vanadium redox flow battery performance using topology optimization. Journal of Power Sources. 2026; 666: 239181. doi: 10.1016/j.jpowsour.2025.239181
2. Wang Y, Lei Z, Wang Z. Performance research in vanadium redox flow battery: Design of serpentine-biomimetic asymmetric flow field configuration. Electrochimica Acta. 2026; 552: 148244. doi: 10.1016/j.electacta.2026.148244

3. Hamrouni C. Recent advances in differential equations, control processes, and secure cryptographic networks for medical data exchange. Advances in Differential Equations and Control Processes. 2025; 32(3). doi: 10.59400/adecp2940
4. Sane AG, Esmaeili M, Rabiee AH. Dual benefits of superhydrophobic surfaces: Suppression of flow-induced vibrations and enhancement of heat transfer in cylindrical structures. Ocean Engineering. 2026; 344: 123643. doi: 10.1016/j.oceaneng.2025.123643
5. Zhang J, Zeng Y, Zhou P, et al. Experimental study on modal characteristics of an underwater rotating disc in coupled nodal circle and diameter modes. Journal of Fluids and Structures. 2026; 140: 104443. doi: 10.1016/j.jfluidstructs.2025.104443
6. Zheng Y, Shi P, Sun Z, et al. Hybrid EXP-FEA-ANN modeling for citrus ripeness detection via modal analysis. Journal of Stored Products Research. 2026; 115: 102801. doi: 10.1016/j.jspr.2025.102801
7. Jiang L, Fan X, Du J, et al. Erosion processes in dry granular rock-ice avalanches with varying ice content: Insights from flume experiments. Engineering Geology. 2026; 363: 108566. doi: 10.1016/j.enggeo.2026.108566
8. Hamrouni J, Khatir Kabashi K, Hamrouni C, et al. Hybrid calculation-estimation modeling for flow field optimization: Enhancing efficiency of biomimetic vanadium redox flow batteries. Advances in Differential Equations and Control Processes. 2026; doi: 10.59400/adecp3793
9. Zheng H, Li M, Wang J, et al. A numerical study on flow-induced vibration of a buoy-mooring system. Marine Structures. 2026; 106: 103975. doi: 10.1016/j.marstruc.2025.103975
10. Park H, Kim ES, Chae EJ, et al. Effect of passive turbulence control parameters on flow-induced vibrations of a circular cylinder. Ocean Engineering. 2026; 349: 124181. doi: 10.1016/j.oceaneng.2026.124181
11. Komuro Y, Uchimichi N, Kondo Y, et al. Development of gas-liquid interfacial velocity correlation for flow-induced vibration analysis of triangular array tube bundle in steam generators. Progress in Nuclear Energy. 2026; 191: 106099. doi: 10.1016/j.pnucene.2025.106099
12. Hamrouni C. Shaping new limits: The future evolution of mathematical models and control strategies. Advances in Differential Equations and Control Processes. 2025; 32(3). doi: 10.59400/adecp2859
13. Hamrouni C, Abdelgader L. Reinforcement learning from demonstration for robust control of superconducting qubits: Decoherence suppression via environmental engineering. Advances in Differential Equations and Control Processes. 2026; doi: 10.59400/adecp3910
14. Zhu H, Shan L, Zhang Y. Flow-induced vibrations of two seal-whisker cylinders in tandem arrangement: A numerical study. Ocean Engineering. 2026; 343: 123109. doi: 10.1016/j.oceaneng.2025.123109
15. Cordero Obando A, Hourigan K, Thompson MC, et al. Flow-induced vibration of an elastically mounted oblate spheroid with variable mass ratio. International Journal of Heat and Fluid Flow. 2026; 117: 110129. doi: 10.1016/j.ijheatfluidflow.2025.110129
16. Lin Y, Li W, Li G, et al. Flow-induced vibration suppression of a square cylinder with Y-shaped jet configuration: Inspired by fish gill structures. Ocean Engineering. 2026; 343: 123338. doi: 10.1016/j.oceaneng.2025.123338
17. Liu Z, Wang Y. Experimental research on a flow-induced vibration piezoelectric energy harvester with downstream interference baffle. Ocean Engineering. 2026; 347: 124052. doi: 10.1016/j.oceaneng.2025.124052
18. Xu Y, Wang Y. Noise analysis and vibration control of flow-induced vibration in the rotating detonation combustor. The Journal of the Acoustical Society of America. 2026; 159(1): 408–421. doi: 10.1121/10.0042234
19. Sun J, Sun R, Qiao P, et al. Numerical study on the mechanism transition characteristics and critical velocity of flow-induced vibration in square tube bundles based on Large Eddy Simulation and quasi-steady theory. Annals of Nuclear Energy. 2026; 227: 112004. doi: 10.1016/j.anucene.2025.112004
20. Dang Z, Chen H, Hugo R, et al. Experimental Study of Two-Phase Flow-Induced Vibrations in Pipelines Under Varying Flow and Burial Conditions. Journal of Fluids Engineering. 2026; 148(1): 011202. doi: 10.1115/1.4069182
21. Jiang Y, Xia B, Chen C, et al. Numerical investigation of excitation mechanism and response behavior of flow-induced vibration in plate-type fuel elements of high-flux reactors cooled by LBE. Annals of Nuclear Energy. 2026; 227: 111983. doi: 10.1016/j.anucene.2025.111983
22. Merzari E, Brockmeyer L, Yuan H, et al. Helical-coil steam generators: Application of computational fluid–structure interaction/flow-induced vibration for heat exchangers and steam generators. In: Steam Generators for Nuclear Power Plants, 2nd ed. Woodhead Publishing; 2026. pp. 673–705.
23. Xiong Z, Wang S, Kang R, et al. Investigation on cross flow induced tube bundle vibration and tube-support contact state. Progress in Nuclear Energy. 2026; 191: 106068. doi: 10.1016/j.pnucene.2025.106068